A Be-W interatomic potential

C Björkas[1], K.O.E Henriksson[2], M Probst[3] and K Nordlund[1]

[1] EURATOM/Tekes, Department of Physics, P.O. Box 43, FI-00014 University of Helsinki, Finland

[2] Department of Chemistry, P.O. Box 55, FI-00014 University of Helsinki, Finland

[3] EURATOM/OEAW, Institute of Ion Physics and Applied Physics, Innsbruck University, 6020 Innsbruck, Austria

E-mail: `carolina.bjorkas@helsinki.fi`

Abstract.

In this work, an interatomic potential for the beryllium-tungsten system is derived. It is the final piece of a potential puzzle, now containing all possible interactions between the fusion reactor materials beryllium, tungsten and carbon as well as the plasma hydrogen isotopes. The potential is suitable for plasma-wall interaction simulations and can describe the intermetallic Be_2W and $Be_{12}W$ phases. The interaction energy between a Be surface and a W atom, and vice versa, agrees qualitatively with *ab initio* calculations. The potential can also reasonably describe Be_xW_y molecules with $x, y = 1, 2, 3, 4$.

Submitted to: *Journal of Physics: Condensed Matter*

1. Introduction

The vast amount of energy released when fusing the hydrogen isotopes deuterium (D) and tritium (T) is, in theory, an ideal energy source. Helium is the only by-product of the process, which requires only small amounts of fuel and is inherently safe [1]. In practise, however, using fusion on a large scale is not easily feasible.

The challenges of a thermonuclear fusion reactor arise from the fact that the fusion fuel is heated up to temperatures ten times higher than that of the Sun's core, thus creating a deuterium-tritium plasma. This plasma is confined and controlled by strong magnetic field in a toroidal chamber called tokamak. Even so, fragments of the plasma will escape the confinement and come in contact with the reactor walls, a phenomenon called plasma-wall interactions (PWI) [2]. These interactions cause, for instance, erosion of the wall material, contamination of the plasma by the eroded species and degradation of the reactor materials.

ITER is an experimental fusion test reactor whose aim is to show that commercial energy can be produced from fusion [3]. The ITER plasma-facing reactor materials have been chosen based on numerous criteria and it will contain beryllium (first wall) and tungsten and carbon (exhaust region, the divertor). As a consequence of the PWI, formation of so called mixed materials is expected. These are alloys of unknown composition and properties. The mixing can cause surprising material changes possibly leading to sudden machine failures. For instance, the mixing caused a tungsten crucible to melt at only 1500 K, effectively destroying the oven used in the experiments [4]. The crucible was in contact with molten beryllium and upon formation of BeW layers, the melting point was greatly reduced. Pure W melts at about 3700 K. This served as an awakening example of the importance of understanding the mixed materials, especially tungsten beryllides.

Gaining this understanding requires studying the materials when situated in a harsh environment. Experiments are extremely useful, but insight into the fundamental reactions, thus allowing for extrapolation to situation not reproducible in today's devices, can be provided only by computer simulation techniques. One such technique is molecular dynamics simulations, which have proven very helpful in understanding different PWI processes for instance by identifying the swift chemical sputtering mechanism in the low energy bombardment of carbon and beryllium [5, 6, 7]. However, the simulations require accurate potentials for every atomic interaction in the system of interest.

In this work, we finalize the task of creating such interatomic potentials for the whole Be-C-W-H system by creating an analytical bond-order potential (ABOP) for Be-W that can be combined with the earlier Be-C-H [8] and W-C-H [9, 10] potentials. Being the first potential for the Be-W system, it serves as a starting shot for comprehensive PWI simulations.

2. Method

2.1. Potential formalism

The potential formalism used originates from the concept of bond order proposed by L. Pauling [11] and it has been shown [12] to resemble both the tight-binding [13] and the EAM

schemes [14, 15]. It has been described extensively elsewhere (in e.g. [12, 16]), so only a brief overview will be given in what follows.

The total energy E of the system is expressed as a sum over individual bond energies, as

$$E = \sum_{i>j} f_{ij}^c(r_{ij}) \left[V_{ij}^R(r_{ij}) - \underbrace{\frac{b_{ij} + b_{ji}}{2}}_{b_{ij}} V_{ij}^A(r_{ij}) \right]. \tag{1}$$

V_{ij}^R and V_{ij}^A are the repulsive and attractive terms, respectively. These are pair potentials of a Morse-like form,

$$V^R(r) = \frac{D_0}{S-1} \exp\left(-\beta\sqrt{2S}(r - r_0)\right),$$
$$V^A(r) = \frac{SD_0}{S-1} \exp\left(-\beta\sqrt{2/S}(r - r_0)\right), \tag{2}$$

where D_0 and r_0 are the bond energy and length of the dimer molecule, respectively and S is an adjustable parameter. β is also related to the dimer, since this can be determined from its ground state oscillation frequency, according to

$$\beta = k\frac{2\pi c}{\sqrt{2D_0/\mu}}, \tag{3}$$

where k is the wave number and μ the reduced mass of the dimer. Through the cut-off function f_{ij}^c the interaction range is restricted,

$$f^c(r) = \begin{cases} 1, & r \leq R - D, \\ \frac{1}{2} - \frac{1}{2}\sin\left(\frac{\pi}{2}(r - R)/D\right), & |R - r| \leq D, \\ 0, & r \geq R + D. \end{cases} \tag{4}$$

Here, R and D are parameters determining the cutoff range and interval. b_{ij} in Equation (1) is the bond order term, which includes three-body interactions and angularity,

$$b_{ij} = (1 + \chi_{ij})^{-\frac{1}{2}}, \tag{5}$$

where,

$$\chi_{ij} = \sum_{k(\neq i,j)} f_{ik}^c(r_{ik}) g_{ik}(\theta_{ijk}) e^{2\mu_{ijk}(r_{ij} - r_{ik})}. \tag{6}$$

μ_{ik} is a fitting parameter and the angular function g_{ik} is of the form

$$g(\theta) = \gamma\left(1 + \frac{c^2}{d^2} - \frac{c^2}{d^2 + (h + \cos\theta)^2}\right), \tag{7}$$

where γ, c, d and h are adjustable parameters.

For making the potential suitable for high energy simulations, a repulsive potential was added as explained in the Appendix.

2.2. DFT calculations

2.2.1. The fitting database The tungsten-beryllium phase diagram includes one clearly identifiable intermetallic phase: the hexagonal Laves Be_2W as well as two narrow phases with the stoichiometry $Be_{12}W$ and $Be_{22}W$ [17] (see figure 1). Formation of Be_2W and $Be_{12}W$ have been observed during experiments in the Be-W system, e.g. [18, 19, 20, 21].

For the fitting of the ABOP potential, *ab initio* density functional theory (DFT) calculations for the caesium chloride (CsCl), rock salt (NaCl), zinc blende (ZnS) and hexagonal Laves Be_2W structures were done. The results of these calculations, including bulk properties such as the equilibrium lattice parameter, bulk modulus and elastic constants, can be seen in table 2. For the binding energy, bond length and vibration frequency ω of the Be-W dimer, calculations from [22] were used, see table 3.

The DFT calculations used the projector augmented wave (PAW) method [23] in a plane-wave basis set as implemented in the Vienna Ab initio Simulation Package (VASP) [24, 25, 26, 27, 28]. Pseudopotentials at the level of the Generalized Gradient Approximation (GGA) developed by Perdew and Wang [29, 30] were used. These were taken from the database supplied with VASP. In the metallic pseudopotentials for Be and W the *s* and *p* states, respectively, were treated as valence states.

The sampling of *k* points in the Brillouin zone was done with the Monkhorst-Pack scheme [31]. The integration over the Brillouin zone was carried out with the Methfessel-Paxton method [32] when relaxing structures, and the linear tetrahedron method of Blöchl *et al.* [33] to obtain accurate energies of relaxed structures. For the simple binary phases CsCl, NaCl and ZnS an energy cutoff of 700 eV was used. The density of *k*-points was 15 in this case. For Be_2W and pure bcc W an energy cutoff of 600 eV and a *k*-point density of 13 was used.

The calculations used an accuracy threshold of 10^{-5} eV = 0.01 meV per atom. In general, properties like the equilibrium cohesive energy, volume, and bulk modulus were calculated by fitting the energy-volume curve to appropriate functions, like the Morse potential or a third order polynomial.

2.2.2. BeW dimer and molecules The Be-W dimer calculations in [22] used the VASP code with the same basis-set and pseudopotentials as described above. A supercell with a border length of 11 Å was used and the energy cutoff for the plane waves was 400 eV and a *k*-point density of 5 was used.

Additionally we performed nonperiodic calculation on Be_xW_y molecules using the B3LYP functional which is very widely employed for molecular calculations. These calculations were performed with the gaussian 03 program. For a better comparison, three basis sets, CEP-121, SDD and LANL2DZ were used [34, 35, 36]. All three gave similar results.

3. Results and discussion

3.1. Be-W according to the ABOP

The potential parameters were found by searching for parameters that reproduce as many properties of structures included in the fitting database as possible. When a satisfactory set was found, the potential was tested against properties not included in the first automatized step (for instance all properties of the Be_2W and $Be_{12}W$ structures), and if not performing adequately, a new parameter set was investigated. Numerous iterations were necessary and compromises were unavoidable.

The agreement of the Be-W potential with the fitting data is seen in table 2. The scarce experimental data to compare to make a comprehensive evaluation difficult. However, the two most important phases Be_2W and $Be_{12}W$ are stable and described reasonably by the potential.

As suggested by the DFT calculations and the phase digram, no stable structure at the stoichiometry 1:1 exists, which we ensured by giving the NaCl and ZnS structure a positive heat of formation (HOF) within the potential. CsCl has a negative HOF according to the ABOP, however, it is dominated by the Be_2W structure and is therefore only metastable. (The existence of a metastable CsCl Be-W has been proposed [17].) In the calculations of the formation energy, the following elemental cohesive energies were used. $E_{DFT}(Be) = -3.71$ eV/atom, $E_{ABOP}(Be) = -3.62$ eV/atom [8] and $E_{DFT}(W) = -12.79$ eV/atom, $E_{ABOP}(W) = -8.89$ [9].

The melting point of Be_2W and $Be_{12}W$ was determined by simulating a solid-liquid interface at zero pressure and different temperatures [37]. The melting temperature was defined as the temperature at which the system was in equilibrium, i.e. when the fractions of solid and liquid parts remained constant. This way, Be_2W melts around 2100 K but the melting point of $Be_{12}W$ was difficult to determine. Above 1300 K, the liquid part was seen to grow at the expense of the crystalline part, but below this temperature, no change at the solid-liquid interface took place for 0.75 ns. This indicates that the crystallization of such a complex phase is very slow and would require lengthy simulations to occur. Therefore we estimate the melting point of $Be_{12}W$ to be ≤ 1300 K.

We also ensured that there were no false minima present at the Be:W = 2:1 concentration by slowly quenching a random melt, consisting of Be and W atoms with that particular Be:W ratio, to zero Kelvin. The final structure was amorphous and higher in energy than the hexagonal Laves Be_2W phase.

The structure and energies of small Be_xW_y molecules were calculated, resulting in the data found in table 3 together with related DFT data. According to the DFT calculations using VASP [22] and the ABOP, the dimer is quite strongly bonded, which is not the case for the DFT calculations of this work. The reason for the discrepancy is not clear but might be related to different functionals and/or methods used in the calculations. The bond lengths are, however, similar.

The properties of the BeW_y molecules according to ABOP are in good agreement with the DFT calculations, but the energies of the Be_xW ones differ with a factor of two. Also,

contrary to DFT results, the linear BeW_2 molecule is stable within the ABOP.

3.2. Interaction energies

The interaction of a slab of hcp Be and a W atom at different distances from the (0001) surface of the slab is defined as

$$\Delta E = E(\text{Be cell} + \text{W atom}) - E(\text{Be cell}) - E(\text{W}). \tag{8}$$

The same definition is used for the reversed situation, i.e. a Be atom interacting with (001) bcc W. In [38, 20], where this interaction has been studied with DFT methods, $E(\text{W})$ and $E(\text{Be})$ is the energy of a free W and Be atom, respectively. In classical MD, this energy is always zero, so that the interaction energy equals $E(\text{Be cell} + \text{W atom}) - E(\text{Be cell})$ (and vice versa).

The calculations of ΔE was done by fixing the z-position of the impurity atom (Be or W), beginning from a distance well above the surface and going to a few monolayers inside the bulk. No restrictions were set for the x and y-position of the atom nor for any of the coordinates of the bulk atoms (except for atoms in the two fixed layers at the bottom of the cell). Full relaxation of the lattice at zero K was hence allowed. The Be slab consisted of 4992 atoms and the W slab of 1280 atoms.

Figure 2 shows the resulting interaction energies. According to the ABOP, Be is exhibiting a potential barrier of about 4.6 eV when penetrating the surface. (This barrier is defined as difference between the minimum and maximum energy.) According to the DFT calculations by A. Allouche [20], this barrier is 3.6 eV. It is also seen that further penetration into the W bulk is not energetically favourable, since the interaction energy is nearing positive values.

The situation is a bit different when looking at how a W atom interacts near a Be surface. Now, the barrier the W encounters when entering the first monolayer is very small: according to the ABOP it is less than 0.8 eV while the DFT barrier is 1.6 eV. The barriers of moving deeper into the bulk are low and the interaction energy negative, so that a W can relatively easily diffuse into Be.

Qualitative agreement between the ABOP and DFT-calculations are thus found: Diffusion of W into Be is easier than the reverse situation. In [20], this was related to experimental observations showing that only very thin films of Be are formed on a W surface.

4. Conclusions

A tool for modeling plasma-surface processes containing both beryllium and tungsten is here provided, since the potential derived in this work is able to describe several Be-W phases. The interaction energy of a Be atom near a W surface and vice versa, is qualitatively similar to DFT calculations, showing that diffusion of Be into bulk W is not energetically favourable. The opposite is true for the reversed system.

Appendix A. Modification of the repulsive potential

The repulsive part of the potentials was modified in a manner previously used for Tersoff-like many body potentials [12, 39]: A total potential V_{Tot} was constructed by joining the original universal ZBL repulsive potential $V_{ZBL}(r)$ [40] with the equilibrium potential $V_{Eq}(r)$ using

$$V_{Tot}(r) = V_{ZBL}(r)(1 - F(r)) + V_{Eq}(r)F(r), \tag{A.1}$$

where V_{Eq} is the potential for states close to equilibrium described in the main text and the Fermi function

$$F(r) = \frac{1}{1 + e^{-b_f(r - r_f)}}. \tag{A.2}$$

Note that the Fermi function is used here merely as a function which smoothly goes from 1 to 0 in a relatively narrow r interval, with no connection to the Fermi level of the electrons of the solid. The value of the constants b_f and r_f are manually chosen so that the potential is essentially unmodified at the equilibrium and longer bonding distances, and that a smooth fit at short separations with no spurious minima is achieved for all realistic coordination numbers. The parameters for each potential are found in table 1.
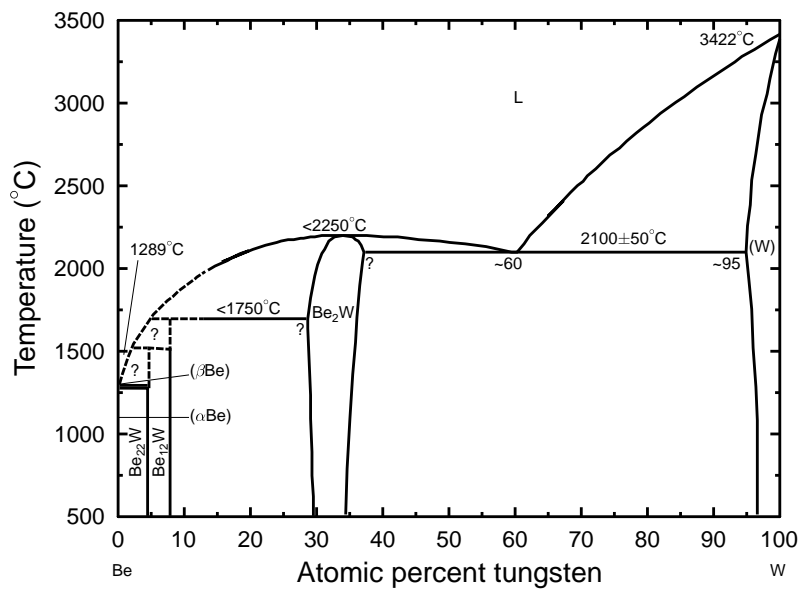
Figure 1. The Be-W phase diagram reproduced from [41].
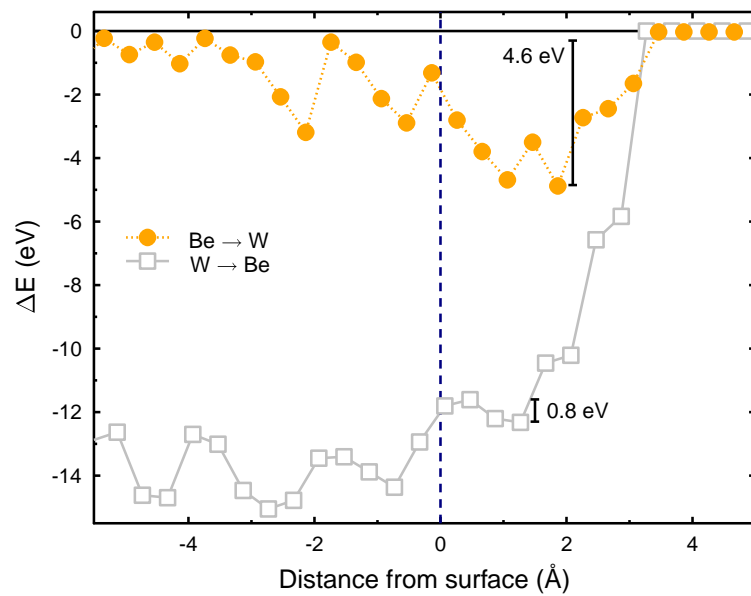
Figure 2. The interaction energy between a slab of bcc (001) W and a Be atom as well as the energy between hcp (0001) Be and a W atom.

Tables and table captions

Table 1. Parameter sets for the different interaction types. The Be-Be parameters are taken from [8] (set II) and the W-W from [9].

	Be-Be	W-W	Be-W
D_0 (eV)	1.03571	5.41861	3.79097878993
r_0 (Å)	2.07880	2.34095	2.06330081049
β (Å^{-1})	1.3	1.38528	0.91209070485
S	1.88982	1.92708	2.29285247962
γ	8.19587×10^{-7}	1.88227×10^{-3}	$2.17149597670 \times 10^{-1}$
c	89.3894	2.14969	34.3953715887
d	0.27443	0.17126	554.148353798
h	0.7606934	-0.27780	-0.8660
R (Å)	2.535	3.10[a]	3.30
D (Å)	0.15	0.10[a]	0.2
2μ	0.0	0.458764	1.2
r_f	0.8	1.3	1.3
b_f	15	12	13

[a] The published cutoff $R = 3.5$ and $D = 0.3$ in [9] is not suitable for ZnS and NaCl BeW.

[1] J. Wesson. *Tokamaks*. Number 48 in Oxford Engineering Series. Clarendon Press, Oxford, 2nd edition, 1997.

[2] R. Parker, G. Janeschitz, H.D. Pacher, D. Post, S. Chiocchio, G. Federici, P. Ladd, ITER Joint Central Team, and Home Teams. Plasma-wall interactions in iter. *Journal fo Nuclear Materials*, 241-243:1–26, 1997.

[3] *The ITER Organization* http://www.iter.org/.

[4] R. P. Doerner, M. J. Baldwin, and R.A. Causey. Beryllium-tungsten mixed-material interactions. *Journal of Nuclear Materials*, 342:63, 2005.

[5] K. Nordlund, E. Salonen, A. V. Krasheninnikov, and J. Keinonen. Swift chemical sputtering of covalently bonded materials. *Pure and Applied Chemistry*, 78(6):1203–1212, 2006.

[6] P. S. Krstic, C. O. Reinhold, and S. Stuart. Chemical sputtering from amorphous carbon under bombardment by deuterium atoms and molecules. *New J. Phys.*, 9:209, 2007.

[7] C. Björkas, K. Vörtler, K. Nordlund, D. Nishijima, and R. Doerner. Chemical sputtering of Be due to D bombardment. *New Journal of Physics*, 11:123017, 2009.

[8] C. Björkas, N. Juslin, H. Timko, K. Vörtler, K. Henriksson, K. Nordlund, and P. Erhart. Interatomic potentials for be, be-c and be-h. *Journal of Physics: Condensed Matter*, 21:445002, 2009.

[9] N. Juslin, P. Erhart, P. Träskelin, J. Nord, K. O. E. Henriksson, K. Nordlund, E. Salonen, and K. Albe. Analytical interatomic potential for modelling non-equilibrium processes in the w-c-h system. *J. Appl. Phys.*, 98:123520, 2005.

[10] D. W. Brenner. Empirical potential for hydrocarbons for use in simulating the chemical vapor deposition of diamond films. *Phys. Rev. B.*, 42:9458, 1990.

[11] L. Pauling. *The nature of the chemical bond*. Cornell University Press, Ithaca, third edition, 1960.

[12] K. Albe, K. Nordlund, and R. S. Averback. Modeling metal-semiconductor interaction: Analytical bond-order potential for platinum-carbon. *Phys. Rev. B*, 65:195124, 2002.

[13] F. Cleri and V. Rosato. Tight-binding potentials for transition metals and alloys. *Phys. Rev. B*, 48(1):22, 1993.

[14] M. S. Daw and M. I. Baskes. Embedded-atom method: Derivation and application to impurities, surfaces, and other defects in metals. *Physical Review B*, 29:6443–6453, 1984.

Table 2. Properties of the beryllium tungsten bulk phases (both hypothetical and existing ones) as obtained from experiments, DFT calculations, and using the analytical potential derived in this work. The notation is as follows. a: lattice parameter, E_{coh}: cohesive energy, ΔH_f: Enthalpy of formation, B: bulk modulus, B': pressure derivative of the bulk modulus.

	Experiment	DFT	ABOP
Zinc blende (ZnS, B3, F$\bar{4}$3m, no. 216)			
a (Å)		5.04	5.29
E_{coh} (eV/f.u.)		-12.42	-9.72
ΔH_f (eV/f.u.)		+4.08	+2.78
Rock salt (NaCl, B1, Fm$\bar{3}$m, no. 225)			
a (Å)		4.61	4.79
E_{coh} (eV/f.u.)		-15.72	-11.86
ΔH_f (eV/f.u.)		+0.77	+0.65
Caesium chloride (CsCl, B2, Pm$\bar{3}$m, no. 221)			
a (Å)		2.90	2.95
E_{coh} (eV/f.u.)		-15.86	-14.34
ΔH_f (eV/f.u.)		+0.32	-1.83
Be$_2$W (MgZn$_2$, C14, P6$_3$/mmc, no. 194)			
a (Å)	4.46[a]	4.46	4.60
c/a	1.63[a]	1.645	1.63
x_1		-0.169884	-0.174
z_2		0.0668	0.0598
E_c (eV/f.u.)		-21.11	-20.88
ΔH_f (eV/f.u.)		-0.61	-4.8
B (GPa)		224.6	167.3
B'		4.34	3.88
C_{11} (GPa)		451	259
C_{12} (GPa)		98	125
C_{13} (GPa)		107	118
C_{33} (GPa)		436	265
C_{44} (GPa)		170	61
T$_{melt}$ (K)	2523[a]		2100±100
Be$_{12}$W (Mn$_{12}$Th, D2$_b$, no. 139)			
a (Å)	7.362[a]	7.260[b]	7.55
c/a	0.573[a]	0.566[b]	0.53
x_1			0.365
x_2			0.280
E_c (eV/f.u.)		-40.56[b]	-63.05
ΔH_f (eV/f.u.)			-10.7
B (GPa)			355.9
B'			-4.1
C_{11} (GPa)			536
C_{12} (GPa)			177
C_{13} (GPa)			268
C_{33} (GPa)			704
C_{44} (GPa)			228

[a] [17]

[b] [38]

[15] D. Brenner. Relationship between the embedded-atom method and tersoff potentials. *Phys. Rev. Lett.*, 63:1022, 1989.

[16] J. Nord, K. Albe, P. Erhart, and K. Nordlund. Modelling of compound semiconductors: Analytical bond-order potential for gallium, nitrogen and gallium nitride. *Journal of Physics: Condensed Matter*, 15(32):5649–5662, 2003.

[17] B. Predel. Be-w (beryllium-tungsten). volume 5b of *Landolt-Börnstein, New Series IV*. SpringerMaterials. DOI: 10.1007/10040476_528.

[18] M.J. Baldwin, R.P. Doerner, D. Nishijima, D. Buchenauer, W.M. Clift, R.A. Causey, and K. Schmid. Be-w alloy formation in static and divertor-plasma simulator experiments. *Journal of Nuclear Materials*, 363-365:1179–1183, 2007.

[19] Ch. Linsmeier, K. Ertla, J. Roth, A. Wiltnera, K. Schmida, F. Kosta, S.R. Bhattacharyyaa, M. Baldwin, and R.P. Doerner. Binary beryllium-tungsten mixed materials. *Journal of Nuclear Materials*, 363-365:1129–1137, 2007.

[20] A. Allouche, A. Wiltner, and Ch. Linsmeier. Quantum modeling (dft) and experimental investigation of beryllium-tungsten alloy formation. *J. Phys.:Condensed Matter*, 21:355011, 2009.

[21] A. Wiltner and Ch. Linsmeier. Surface alloying of thin beryllium films on tungsten. *New Journal of Physics*, 8:181, 2006.

[22] K. Vörtler, 2007. Special assignment of the course "Introduction to Electronic Structure Calculations".

[23] P. E. Blöchl. Projector augmented-wave method. *Phys. Rev. B*, 50(24):17953–17979, 1994.

[24] G. Kresse and J. Hafner. Ab initio molecular dynamics for liquid metals. *Phys. Rev. B*, 47(1):558–561, 1993.

[25] G. Kresse and J. Hafner. Ab initio molecular-dynamics simulation of the liquid-metal-amorphous-semiconductor transition in germanium. *Phys. Rev. B*, 49(20):14251–14269, 1994.

[26] G. Kresse and J. Furthmüller. Efficiency of ab-initio total energy calculations for metals and semiconductors using a plane-wave basis set. *Comp. Mater. Sci.*, 6:15–50, 1996.

[27] G. Kresse and J. Furthmüller. Efficient iterative schemes for ab initio total-energy calculations using a plane-wave basis set. *Phys. Rev. B*, 54(16):11169–11186, 1996.

[28] G. Kresse and D. Joubert. From ultrasoft pseudopotentials to the projector augmented-wave method. *Phys. Rev. B*, 59(3):1758–1775, 1999.

[29] J. P. Perdew, J. A. Chevary, S. H. Vosko, K. A. Jackson, M. R. Pederson, D. J. Singh, and C. Fiolhais. Atoms, molecules, solids, and surfaces: Applications of the generalized gradient approximation for exchange and correlation. *Phys. Rev. B*, 46(11):6671–6687, 1992.

[30] Y. Wang and J. P. Perdew. Correlation hole of the spin-polarized electron gas, with exact small-wave-vector and high-density scaling. *Phys. Rev. B*, 44(24):13298–13307, 1991.

[31] H. J. Monkhorst and J. D. Pack. Special points for brillouin-zone integrations. *Phys. Rev. B*, 13(12):5188–5192, 1976.

[32] M. Methfessel and A. T. Paxton. High-precision sampling for brillouin-zone integration in metals. *Phys. Rev. B*, 40(6):3616–3621, 1989.

[33] P. E. Blöchl, O. Jepsen, and O. K. Andersen. Improved tetrahedron method for brillouin-zone integrations. *Phys. Rev. B*, 49(23):16223–16233, 1994.

[34] P. J. Hay and W. R. Wadt. Ab initio effective core potentials for molecular calculations - potentials for the transition-metal atoms sc to hg. *J. Chem. Phys.*, 82:270–283, 1985.

[35] D. Andrae, U. Haeussermann, M. Dolg, H. Stoll, and H. Preuss. Energy-adjusted ab initio pseudopotentials for the 2nd and 3rd row transition-elements. *Theor. Chem. Acc.*, 77:123–141, 1990.

[36] W. J. Stevens, M. Krauss, H. Basch, and Can. J. P. G. Jasien. Relativistic compact effective potentials and efficient, shared-exponent basis-sets for the 3rd-row, 4th-row, and 5th-row atoms. *Can. J. Chem.*, 70:612–630, 1992.

[37] J. R. Morris, C. Z. Wang, K. M. Ho, and C. T. Chan. Melting line of aluminum from simulations of coexisting phases. *Phys. Rev. B*, 49(5):3109, 1994.

[38] A. Allouche and Ch. Linsmeier. Quantum study of tungsten interaction with beryllium. *J. Phys.:Conference Series*, 117:012002, 2008.

[39] C. Björkas and K. Nordlund. Comparative study of cascade damage in Fe simulated with recent potentials. *Nuclear Instruments and Methods in Physics Research B*, 259:853–860, 2007.

[40] J. F. Ziegler, J. P. Biersack, and U. Littmark. *The Stopping and Range of Ions in Matter*. Pergamon, New York, 1985.

[41] H. Okamoto and L. E. Tanner. In S.V. Nagendra Naidu and P. Ramo Rao, editors, *Phase Diagrams of Binary Tungsten Alloys*. Indian Institute of Metals, Calcutta, 1991.

Table 3. Properties of Be-W molecules according to DFT and the ABOP. The Be-W-Be angle in Be_4W and W-Be-W in BeW_4 molecules is 90°.

molecule	DFT		ABOP
	[22]	This work	
BeW			
r_{Be-W} (Å)	2.11	2.062	2.12
E (eV)	-3.78	-1.71	-3.74
ω (cm^{-1})	480	570	454
BeW_2 linear			
r_{Be-W} (Å)		–	2.11
E (eV)		unstable	-6.96
BeW_2 non-linear			
r_{Be-W} (Å)		2.229	2.21
E (eV)		-10.97	-10.58
θ (°)		58.0	61.8
BeW_3			
r_{W-W} (Å)		2.333	2.33
r_{Be-W} I (Å)		2.242	2.36
r_{Be-W} II (Å)		2.339	3.84
E (eV)		-16.06	-17.84
BeW_4			
r_{Be-W} (Å)		1.871	1.93
E (eV)		-17.68	-20.70
Be_2W linear			
r_{Be-W} (Å)		2.132	2.11
E (eV)		-3.94	-6.96
Be_2W non-linear			
r_{Be-W} (Å)		2.115	2.12
E (eV)		-3.94	-7.61
θ (°)		63.7	59.3
Be_3W			
r_{Be-Be} (Å)		2.355	2.12
r_{Be-W} I (Å)		2.127	2.17
r_{Be-W} II (Å)		2.098	2.20
E (eV)		-6.04	-11.12
Be_4W			
r_{Be-W} (Å)		2.172	2.17
E (eV)		-7.24	-12.31